Flow field measurements of the grinding cooling liquid jet

Björn Espenhahn[1,*], Lukas Schumski[2], Dirk Stöbener[1,3], Daniel Meyer[2,3], Andreas Fischer[1,3]

1: Bremen Institute for Metrology, Automation and Quality Science (BIMAQ), University of Bremen, Germany
2: Dept. of Manufacturing Technologies, Leibniz-Institute for Materials Engineering (IWT), Germany
3: MAPEX Center for Materials and Processes, University of Bremen, Germany
*Corresponding author: B.Espenhahn@bimaq.de

Keywords: PIV processing, grinding, two-phase flow analysis, optical disturbances, systematic measurement deviation

ABSTRACT

The workpiece cooling by metalworking fluids, which has a significant influence on the workpiece surface layer quality, is not fully understood for industrial grinding processes. This necessitates significant effort in determining optimal cooling conditions empirically, raising part manufacturing costs. As a solution, a measurement method for the metalworking fluid flow field near the grinding wheel is desired to close the knowledge gap. However, the fluctuating curved surfaces of the coolant cause unpredictable in light deflections and reflections, making optical flow measurements difficult. To determine the effect of light deflection, non-invasive measurement of the light deflection of the two-phase flow is required. We present flow measurements of the cooling process in grinding for in-process supply conditions, with the focus on measurability and reliability of the whole flow process, at first without a working piece. To investigate the yet unknown optical measurement deviations due to light refraction, Particle Image Velocimetry is applied in a grinding machine in combination with a Background oriented Schlieren. To evaluate the impact of light deflection on the flow measurements, the underlying theoretical principles of a ray-tracing approach are derived, to relate the non-invasive observation through the two-phase flow to the light refraction for measurement inside the flow. As a result, for the nozzle flow, a systematic measurement deviation of up to 2% is identified and after the correction, a plausible flow behaviour is obtained. Further in-situ measurements of the coolant flow in interaction with the grinding wheel reveal a detailed description of the fluid-workpiece interaction.

1. Introduction

Grinding is an important manufacturing process in creating high-quality surfaces, e.g., for refractive and reflective optical components. The grinding process is typically cooled with a metalworking fluid (MWF), which is projected via a nozzle onto the grinding wheel and workpiece to reduce the temperature and to prevent unwanted grinding burn (Brinksmeier et al., 2006). Investigations show that the interaction of the coolant with tool and workpiece strongly depends on the supply conditions (nozzle shape, inflow angle and nozzle exit velocity), but the actual fluid

dynamics have not yet been taken into account since flow measurements are not available (Meyer and Wagner, 2016). For an efficient design of the grinding cooling process, however, a qualitative and quantitative understanding of the cooling liquid flow field is required (Heinzel et al., 2020). First flow measurements with complementary flow visualisation approaches of shadowgraphy and particle image velocimetry (PIV) have been conducted to provide qualitative (Schumski et al., 2022) and quantitative (Espenhahn et al., 2021; Vanselow et al., 2021) insight into the interaction between the cooling liquid flow and the grinding wheel, respectively. The influence of unavoidable light deflections in the two-phase flow on the measurement error and, if necessary, a respective error correction have not been investigated so far, which are essential requirements towards reliable flow measurement results. The light deflections at the coolant supply jet depend on the free-jet geometry, which changes significantly depending on the flow conditions. Consequently, it is required to investigate the effect of light deflections for various nozzle exit velocities of the free jet, i.e. flow regimes ranging from laminar to turbulent.

The impact of light deflections on PIV measurements is described by Elsinga et al. (2005), who derived a relation for the velocity error caused by the particle position error due to light refraction. Therefore, a correction of the systematic velocity error is possible with a determination of the local particle position error. Various approaches have been developed to compensate the influence of light deflections at fluid flows. With the help of ray-tracing and a known surface geometry of the phase transition (Minor et al., 2007), flow measurements have been carried out in, for example, droplets (Kumar et al., 2017) or a super-cavity (Wu et al., 2019). For the correction of the optical distortion on the liquid jet flow for grinding, a model of the surface geometry of the liquid is necessary, which is not measurable for the turbulent supply flow in grinding so far. An alternative method is to use adaptive optics in combination with artificial intelligence (AI) trained algorithms to minimise optical distortions. With this approach, the influence of light deflection can be corrected in real time via reference measurements. For example, with the use of a Fresnel guiding star, the influence of randomly fluctuating surfaces was corrected for μPIV-measurements (Gao et al., 2021). While this is a promising approach, it is not applicable for measurements in a state-of-the-art grinding machine, mainly due to the fast fluctuating jet surface.

A more simple approach to determine the impact of optical distortions is Background Oriented Schlieren (BOS). BOS quantifies the influence of light deflection by observing deflection depending changes of a reference image (Richard and Raffel, 2001). The changes correspond to the particle position deviations as they appear in PIV measurements. Using BOS, a determination and correction of randomly fluctuating inhomogeneous refractive index fields on PIV measurements is shown by C. Vanselow and A. Fischer (2018). For liquid flows, Moisy et al. (2009) proposed a method to measure the local slope of an assumed flat surface with BOS, which was adopted by Ng et al. (2011) for simultaneous measurements of both, flow velocity (with PIV) and surface topography. They demonstrated a proportional relationship between the light deflection and the local surface slope for small slope deformations. Nevertheless, Gomit et al. (2013) pointed out, that for a correction of the PIV measurements, the local light deflection must be known, which is proportional to the curvature of the surface. For the reconstruction of the surface topography an

integration of the surface slope is used, which is highly insecure to outliers. To bypass the use of integration for the surface topography determination of waves in a water tank, they proposed a stereoscopic measurement setup. For this purpose, the apparent particle position error for both camera views with respect to their view angles was evaluated. In addition, a third camera below the tank observing the flow without optical distortions was used as a reference. In the combination of the calibrated views of all three cameras, simultaneous measurements of the flow velocity (by means of PIV) and the surface topography were achieved without the use of integration. As a result, a correction of the light deflections from a known surface topography is shown to be possible. However, the used undisturbed reference image within the measurement plane is not achievable for a PIV measurement inside the liquid free jet used for grinding, as it has no plane surface.

Therefore, we propose a measurement principle to determine the directional derivative of the light deflection for a liquid free jet by means of a BOS-based approach. With the presented approach, the 2d distortion map for the static and randomly fluctuating part of the liquid-air interface of the coolant supply flow is assessed. The distortion map is then used to determine the PIV measurement deviations and, finally after error correction, to obtain valid flow field measurements of the coolant flow generated by a rectangular-shaped orifice of a Rouse-designed nozzle.

In section 2, the underlying theoretical principle for the BOS-based ray tracing approach for the determination of the boundary geometry of a curved liquid jet is discussed. The realisation of this approach is described in section 3. The results are presented and discussed in section 4, beginning with the systematically impacted PIV velocity measurements of the supply flow, followed by the error correction and concluding with additional measurements of the jet flow in interaction with the grinding wheel. Section 5 draws conclusions from the results and provides an outlook for future work.

2. Principles of the methods

The flow field measurements are performed with PIV. Its principle is based on flow visualisation with flow tracers, what allows a flow velocity calculation based on the tracer's motion, while flow-particle slip is neglected. For this purpose, small particles are added into the coolant liquid and illuminated with pulsed laser light. A camera records the positions of the particles and calculates the velocity from the particle shift between two successive images.

Since PIV is an optical flow measurement technique, it suffers from distortions of the optical illumination and the observation path caused by light refraction. As proposed by Elsinga et al. (2005), the systematic deviation $\Delta\vec{U}$ of the flow velocity $\vec{U}$ induced by a refraction depending particle position error $\vec{\xi}$ is

$$\Delta U_i = \left(\frac{\partial \xi_i}{\partial i}\right) \cdot U_i - \left(\frac{\partial U_i}{\partial i}\right) \cdot \xi_i, \tag{1}$$

where $\vec{U}$ is the measured velocity and $i = x, y, z$ denotes the component in the x, y, or z-directions.

As a consequence, the particle position error ξ_i and its directional derivative $\frac{\partial \xi_i}{\partial i}$ in the measurement plane must be measured in addition to the flow velocity field U_i and the directional derivative of the velocity field $\frac{\partial U_i}{\partial i}$ to evaluate the influence of light refraction on the PIV measurement. Since the velocity components and their changes in the y- and z-direction are negligible small, the determination of the refraction-induced systematic velocity deviation ΔU_x can be reduced to the consideration of the x-components of the quantities in Eq. 1.

$$\Delta U_x = \frac{\partial \xi_x}{\partial x} \cdot U_x - \frac{\partial U_x}{\partial x} \cdot \xi_x. \tag{2}$$

To determine the directional derivative $\frac{\partial \xi_x}{\partial x}$ of the particle position error, the free-surface synthetic Schlieren (FS-SS) approach developed by Moisy et al. (2009) is adapted. As reference pattern, a randomly distributed dot pattern is used. The liquid free jet is positioned in between of the reference pattern and the camera. Due to the light refraction of the two-phase flow, a local displacement of the observed dot pattern with respect to the undisturbed reference appears. To quantify the displacement field, each recorded image is processed by means of a section-wise digital image correlation with the undisturbed reference image. The observed displacement Δx is then directly related to $\frac{\partial \xi_x}{\partial x}$, the directional derivative of the particle position error in x-direction, which is derived in the following. The corresponding particle position error ξ_x is calculated by integrating $\frac{\partial \xi_x}{\partial x}$.

The derivation presented hereafter focuses on the light deflections in the observation path of the PIV measurement technique and neglects the deflections of the illumination light. This is feasible since particles in the liquid jet are illuminated with a light sheet of approximately the same thickness as the liquid jet, expecting an illumination of the particles in its entire volume. For the further description of the occurring light deflection for PIV measurements in the free jet as well as the observable deflection of the light passing through the jet, following helpful assumptions of the free jet surface are made:

- The interfaces through which observation is made are self-similar and separated from each other by the liquid jet thickness d, which corresponds to the nozzle outlet height.

- Changes in surface geometry are small in relation to the liquid jet thickness, and surface tilt angles ϑ are small so that $\sin(\vartheta) \approx \tan(\vartheta) \approx \vartheta$.

A graphical representation of the light deflection under these assumptions is shown in Fig. 1. Displayed is the arrangement of a camera, observing a reference pattern at a distance z, whereby the optical path is disturbed at the two surfaces S_1 and S_2 of the liquid jet. The resulting particle position error ξ_x in the measuring plane is caused by the refraction at S_1, which leads to a change of the light direction by the angle δ_1. The observable light deflection Δx in the experiments occurs from the refraction at S_1 and S_2, which causes a change in the light direction by the angle δ_2 and additionally a lateral shift δx. These refraction effects are considered in more detail below. First, the light deflection at surface S_1 is described that affects the PIV measurement. Subsequently, the

observation through the jet is discussed and an expression for the directional derivative of the particle position error $\frac{\partial \xi_x}{\partial x}$ is derived.
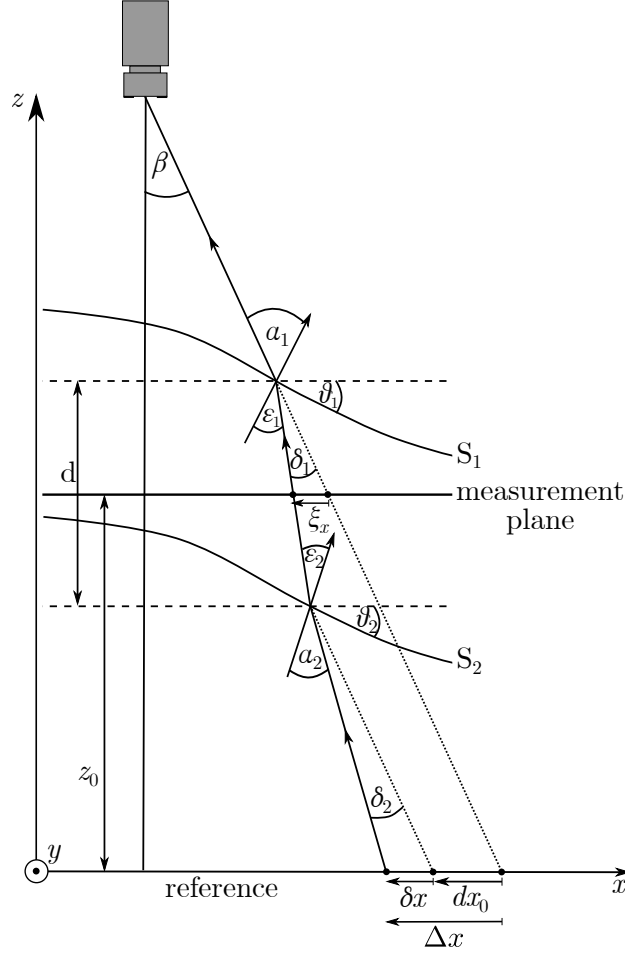

Figure 1. Schematic illustration of light refraction at two self-similar surfaces S_1 and S_2 separated by the jet thickness d, leading to the deflection Δx for a camera, that observes a reference pattern at a distance z with observation angle β, and the particle position error ξ_x in the PIV measurement plane. The dotted lines indicate the undisturbed light paths as they occur without refraction (undisturbed reference) and refraction with assumption of a plane plate and refraction only at surface S_2. α_1 and α_2 represent the angles to the surface normal of S_1 and S_2, respectively, and ε_1 and ε_2 are the corresponding refractive angles, whereby δ_1 and δ_2 depict the change of light direction after refraction at S_1 and S_2. ϑ_1 and ϑ_2 depict the slope of the surface. Note, that the depiction is overdrawn in order to adequately illustrate the influence of light refraction.

According to the theory of Moisy et al. (2009), the particle position error ξ_x can be given as

$$\xi_x \approx \delta_1 \cdot d/2 = \kappa \cdot \alpha_1 \cdot d/2, \tag{3}$$

with α_1 as the angle of the incidence ray to the surface normal of S_1 and $\kappa = 1 - n/n'$ denoting the change of the light ray direction according to Snell's law. n' and n denote the refractive indices of the refractive medium and its surroundings respectively.

$\frac{\partial \xi_x}{\partial x}$ can be calculated accordingly with

$$\frac{\partial \xi_x}{\partial x} = \kappa \cdot \frac{d}{2} \cdot \frac{\partial \alpha_1}{\partial x}. \tag{4}$$

The directional derivative of the particle position error depends on the curvature of S_1 (i.e. the directional derivative of the angle α_1) and scales with the distance from S_1 to the measuring plane, which is approximately $d/2$. To determine ξ_x and $\frac{\partial \xi_x}{\partial x}$, either a measurement of the surface topography of S_1 or a direct measurement of the light deflection within the measurement plane is necessary, which is both not possible for the given conditions.

For this reason, the light deflection within the measurement plane is derived from the deflection measurement of the light passing through both surfaces. The observed deflection through the jet is shifted in comparison to the undisturbed reference by Δx, which is the sum of a constant shift dx_0 and a shift δx due to the changed light direction:

$$\Delta x = dx_0 + \delta x \tag{5}$$

Here, the two summands can be described as the resulting shifts from the refraction on a plane-parallel plate and a dispersive prism, respectively, beginning with the latter.

The displacement δx is caused by a change of the light direction. Its length can be approximated with the angle δ_2 and the distance z_0 between S_2 and the reference pattern according to the aforementioned jet geometry assumptions of small angles:

$$\delta x \approx \delta_2 \cdot z_0. \tag{6}$$

The angle δ_2 results from different slopes of the surface S_1 at the point of the incoming light ray and the surface S_2 at the point of the outgoing light ray. This difference $\vartheta_1 - \vartheta_2$ of the surface tilt angle will be noted as γ. The light deflection angle δ_2 is approximated according to the change of the light direction that appears for a ray passing through a dispersive prism with an apex angle γ:

$$\delta_2 = \alpha_1 + \arcsin\left(\frac{n}{n'}\sin\left[\gamma - \arcsin\left(\frac{n'}{n}\sin\alpha_1\right)\right]\right) - \gamma. \tag{7}$$

Considering a thin thickness of the liquid jet and small slopes, so that each sine and inverse sine expression can be expressed by the function argument, Eq. 7 simplifies to

$$\delta_2 \approx \left(\frac{n'}{n} - 1\right) \cdot \gamma. \tag{8}$$

Inserting Eq. 8 into Eq. 6 and solving for γ leads then to

$$\gamma = \frac{\delta x}{\left(\frac{n'}{n} - 1\right) \cdot z_0}. \tag{9}$$

As a result, the displacement δx can be calculated from a measurement of γ, since the refractive index and the distance z_0 are known.

To derive a relation between the deflection of light in the jet and the deflection of light by the jet, the assumption of self-similarity is used. As given in Eq. 9, changes in the light direction result from a tilt between both surfaces. This tilt is caused by a lateral shift dx_0 of the refraction points of S_1 to S_2, which contains the changes of the surface slope along the direction of the lateral shift and thus relates to the changes of the surface S_1 along the $x-$direction. Therefore, changes of S_1 are equivalent to changes of the refraction angle α_1. Assuming small changes in the surface geometry with respect to the lateral shift, the tilt angle γ is in first order approximation equal to changes of S_1 and α_1, respectively, leading to

$$\gamma \approx \frac{\partial \alpha_1}{\partial x}. \tag{10}$$

Since the relationship between tilt angle and changes of the first surface are established, a substitution of Eq. 9 into Eq. 4 is possible and reveals an equation of the observed light deflection in relation to the change in particle shift in the measurement plane:

$$\frac{\partial \xi_x}{\partial x} = \frac{\kappa \cdot d}{2} \cdot \frac{\delta x}{\left(\frac{n'}{n} - 1\right) \cdot z_0} = \frac{n}{n'} \cdot \frac{d}{2 \cdot z_0} \cdot \delta x. \tag{11}$$

Thus, a relationship for the directional derivative of the particle position deviation was derived for observing δx depending on the light refraction numbers and distance between reference pattern and measurement plane.

To extract the required displacement δx from the measured displacement Δx, the constant lateral displacement dx_0 must be subtracted (Eq. 5). It is assumed that the lateral displacement can be approximated by the refraction on a plane-parallel plate (aligned to the observation plane), so that it can be calculated by

$$dx_0 = d \cdot \sin \beta \cdot \left(1 - \frac{\cos \beta}{\sqrt{(n/n')^2 - \sin^2 \beta}}\right). \tag{12}$$

The refraction at the plane-parallel plate provides for small angles a constant change of the observed displacement in dependency of the observation angle β, the refractive indices n and n' and the thickness of the jet d. With a measurement of Δx and approximation of dx_0, δx can be calculated with the use of Eq. 12. This given, $\frac{\partial \xi_x}{\partial x}$ (and with integration ξ_x) are determined with Eq. 11, and thus the light deflection for the evaluation of Eq. 2 is obtained.

To correct the velocity measurements, the time-averaged light deflection obtained by an observation through the jet is measured for similar flow conditions as for the velocity measurements and the systematic error is determined and corrected according to Eq. 2, leading to the corrected flow velocity $U_{x,\text{cor}}$, with

$$U_{x,\text{cor}} = U_x - \Delta U_x = U_x - \left(\frac{\partial \xi_x}{\partial x} \cdot U_x - \frac{\partial U_x}{\partial x} \cdot \xi_x\right). \tag{13}$$

3. Experimental setup

The measurements are conducted in a surface grinding machine of the type Micro-Cut A8 CNC manufactured by the company ELB with the setup shown in Fig. 2.

The coolant is supplied through a nozzle with a specific profile according to Rouse with a rectangular outlet (width of $20\,\text{mm}$, height of $1.25\,\text{mm}$) onto the grinding wheel surface (Fig. 2b). The used metal working fluid is *CUT MAX 902-10* with a density of $0.82\,\text{kg/m}^3$ and dynamic viscosity of $11\,\text{mm}^2/\text{s}$ at a temperature of $40\,°\text{C}$. The coolant has not been diluted and is a visually transparent yellow-golden liquid with a refractive index of 1.44575 ± 0.00018. The used volume flow is measured with an oval wheel meter with an accuracy of $\pm\, 0.25\,\text{L/min}$. The used grinding wheel has a radius of $200\,\text{mm}$ and rotates with a circumferential velocity of $35\,\text{m/s}$. To provide access for the optical components into the grinding chamber, the protective acrylic glass window that closes the grinding chamber is removed and replaced with a transparent foil (Fig. 2a). Viewing windows are cut into the foil to achieve an undisturbed observation of the volume flows. Work safety is ensured by an external protective housing, which additionally grants laser safety.
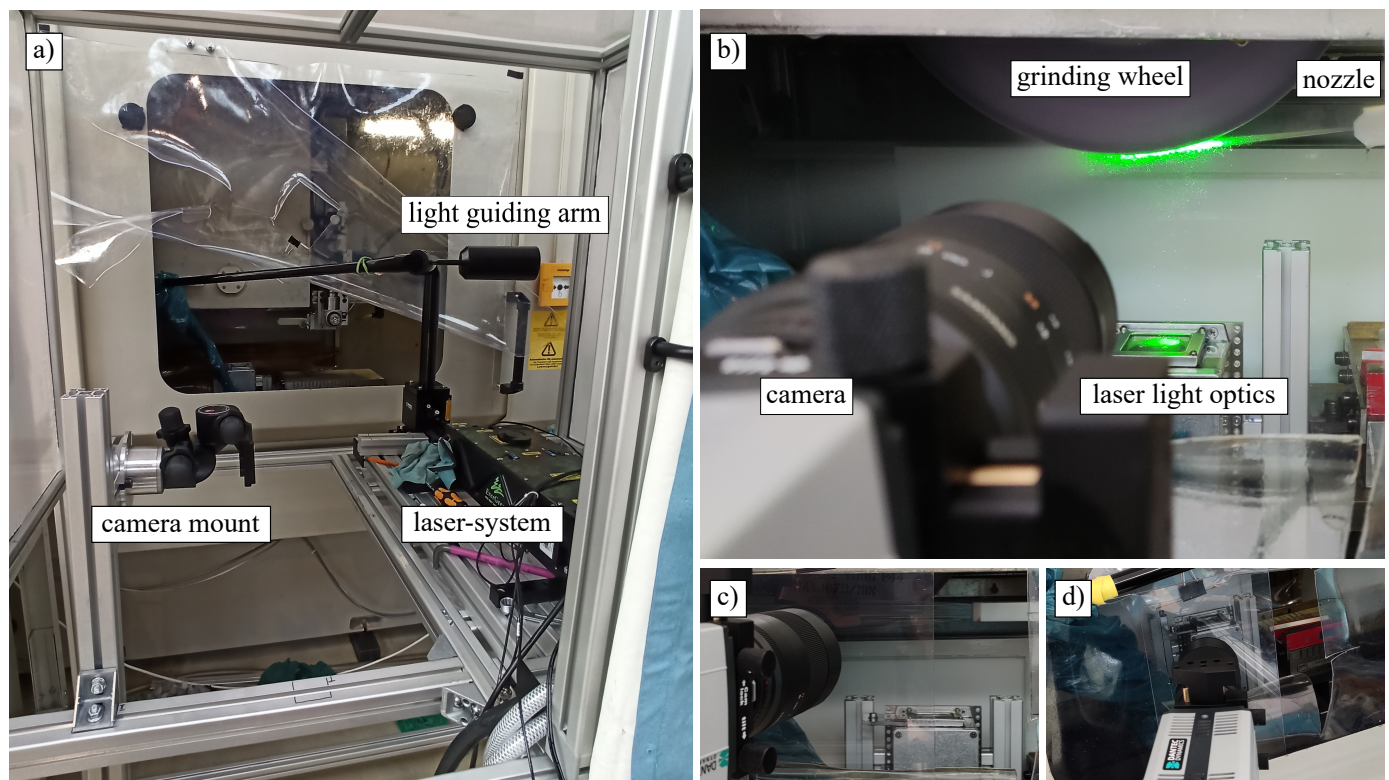

Figure 2. Used experimental flow measurement setup in the grinding machine: a) setup in the protective housing, where the optical components such as the laser, light guiding arm and camera are installed; b) Image of running measurement to show the arrangement of the grinding wheel and nozzle in the grinding machine; c) and d) show the by 12.5° angled arrangement for the supply flow measurements from different perspectives.

To obtain PIV measurements of the coolant supply, polyamid seeding particles with an average size of $50\,\mu\text{m}$ and a density of $1.03\,\text{g/cm}^3$ are filled into the coolant tank of the grinding machine.

To illuminate the seeded flow, a frequency-doubled pumped Nd:YAG pulsed laser at a wavelength of $532\,\text{nm}$ with a maximum energy per pulse of $200\,\text{mJ}$ and a pulse length of $10\,\text{ns}$ of the type Evergreen from the company Quantel is used. A double pulse repetition rate of $15\,\text{Hz}$ with a time separation per pulse between $15\,\mu\text{s}$ to $25\,\mu\text{s}$, which is adjusted according to the flow velocity, serves to capture the fluid flow with a sufficient measurement rate. The laser light sheet has a width of approximately $50\,\text{mm}$ with a sheet thickness of $1\,\text{mm}$. The laser is guided into the grinding machine with a light-guiding arm, that provides the necessary flexibility and protection from contaminating coolant for the optical components. The optics to form a laser light sheet are installed in the grinding machine and protected by a housing to avoid unwanted contamination by coolant droplets (Fig. 2a,b).

For investigating the coolant supply flow, an interaction with the grinding wheel is prevented by moving it out of plane (see Fig. 2c). In order to determine the top view of the coolant free jet flow, the nozzle is rotated by $90°$ instead of reassembling the optical measurement setup. To prevent the influence of reflections when illuminating the free jet, the observation of the camera is tilted by $12.5°$ and a Scheimpflug adapter is used to ensure a uniformly focused observation of the measuring plane (see Fig. 2d). Finally, the nozzle is placed in its original position and the coolant flow interacting with the rotating wheel is studied.

A $5.5\,\text{Mpx}$ sCMOS camera of the type Zyla from the company Andor with a $100\,\text{mm}$ focal length macro objective from the company Samyang is used for all observations. The distances between camera and measurement plane were varied depending on the measurements tasks. Measurements of the supply flow are conducted with a distance of $520\,\text{mm}$, leading to a spatial resolution of $35\,\mu\text{m/px}$. Measurements of the flow in interaction with the grinding wheel were taken at a distance of $540\,\text{mm}$ with a spatial resolution of $39\,\mu\text{m/px}$ and lastly BOS measurements with a distance of $600\,\text{mm}$ result in a spatial resolution of $52\,\mu\text{m/px}$. For BOS-measurements, the randomly distributed dot-pattern is placed at a distance of $z_0 = 5\,\text{mm}$ to the centre of the nozzle outlet.

The calculations of the velocity field as well as the optical displacements during the BOS measurements are carried out with an adaptive PIV algorithm (used software: DynamicStudio, developed by Dantec Dynamics) with an overlap of $75\,\%$ for an interrogation area size of $32\,\text{px} \times 32\,\text{px}$. For each presented result, 1000 single measurements were taken and the averaged velocity field was calculated after automated outlier deletion with a range validation to minimise the residual impact of measurement outliers.

4. Results

Flow measurements of the supply flow are presented and the impact of optical distortions on the flow measurements is discussed in Section 4.1. In Section 4.2, the BOS measurements are presented and used for a correction of the systematic measurement deviations caused by light refraction. Lastly, measurement results of the liquid-tool interacting flow are presented in Section 4.3.

4.1. PIV measurements of supply flow

PIV velocity field measurements are taken for a flow rate of $25\,\text{L/min}$, $30\,\text{L/min}$ and $38\,\text{L/min}$, resulting in a laminar, transient and turbulent flow respectively. Fig. 3 shows the determined flow fields (a, c, e) as well as the raw images (b, d, f) of the recordings for the different flow rates. The flow directions in the images a), c) and e) are indicated by the directions of the plotted vectors and the local magnitude of the 2d flow field $|U|$ in m/s is represented by the colour-coded background. The flow was measured in the range $x = 10\,\text{mm}$ to $70\,\text{mm}$ after the nozzle outlet.
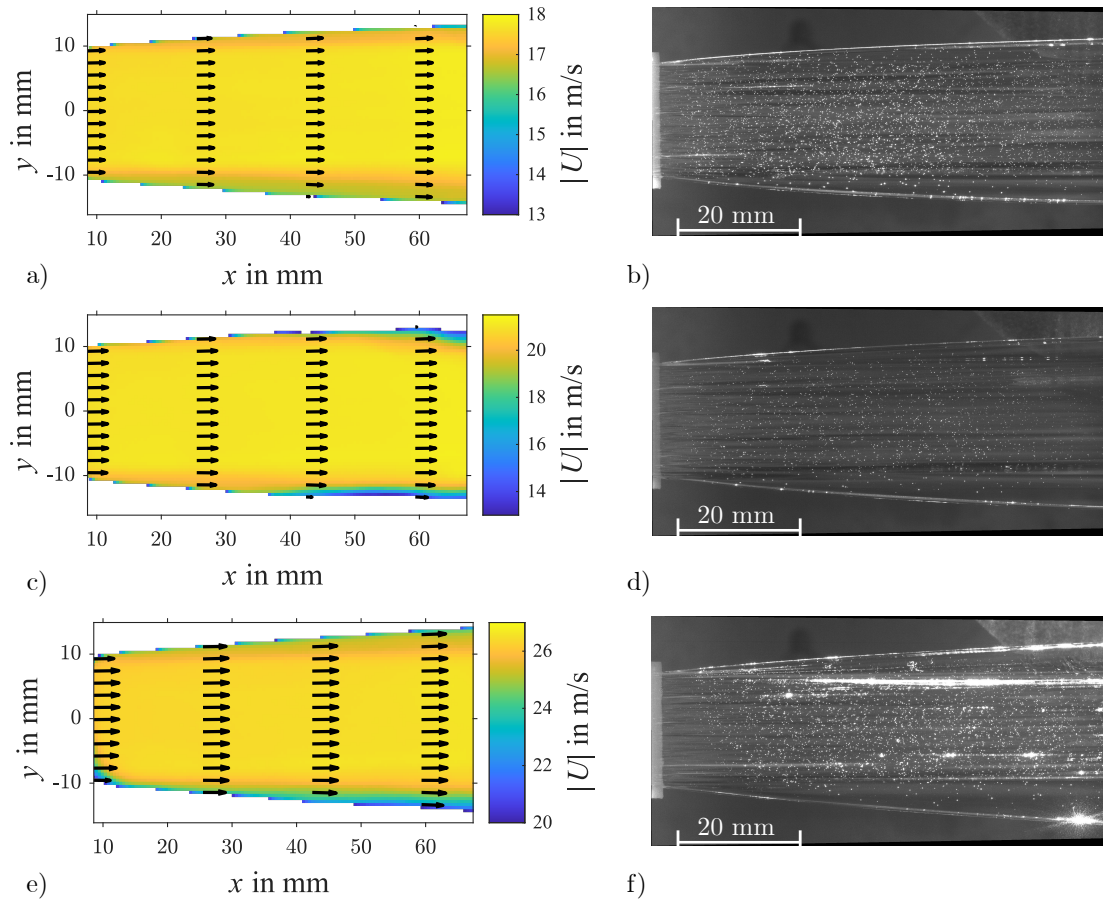

Figure 3. a), c), e) Measured free jet velocities with volume flows of $Q = 25\,\text{L/min},\ 30\,\text{L/min}$ and $38\,\text{L/min}$ with corresponding velocity magnitude $|U|$ in m/s. b), d), f) Calibrated recordings of the visualised flow, achieved with a PIV measurement setup containing a pulsed laser light sheet to illuminate the seeding.

The velocities for all three inflow conditions show a similar behaviour: The flow is strictly monotonic in the central area ($y = -8.5\,\text{mm}$ to $8.5\,\text{mm}$) and shows a strong decrease towards the lateral edges. In the corresponding area of the raw data, the central area can be assessed as a core jet area with a homogeneous velocity. At the lateral edges, a fanning out of the flow can be perceived, which is more pronounced for larger volume flows. The further analysis is focused on the core jet area to depict the nuances of the flow deviations caused by light refraction. For this purpose, the core jet area for each volume flow is averaged along the y-axis and the velocity along the x-axis is shown in Fig. 4. The mean velocities for the three flows at $x = 20\,\text{mm}$ are measured

with $17.64\,\mathrm{m/s}$, $20.98\,\mathrm{m/s}$ and $26.37\,\mathrm{m/s}$. The velocity progression is almost identical for all three volume flows: A weak increase of the velocity along the x-axis can be perceived, whereby minor changes appear at $x = 30\,\mathrm{mm}$ and $x = 50\,\mathrm{mm}$. These are strong indicators of the influence of light refraction on the PIV measurement results, because an increase in velocity is not plausible. Since the effective cross-sections of the flows increase with the distance from the nozzle exit a velocity decrease is expected due to mass conservation. Furthermore, friction with the surrounding air causes an additional decrease in velocity. Consequently, a correction of the velocities is necessary to obtain physically reasonable results.
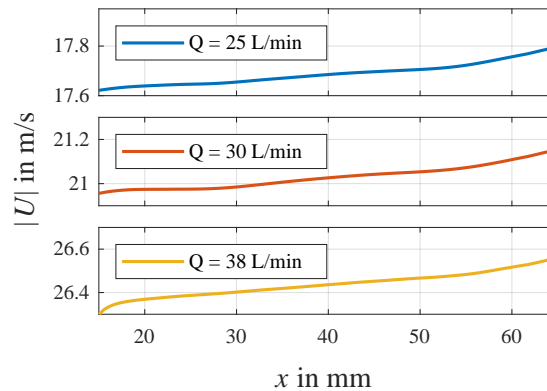

Figure 4. Average flow velocity for the core jet region of $y = -8.5\,\mathrm{mm}$ to $8.5\,\mathrm{mm}$ for the volume flows of $Q = 25\,\mathrm{L/min}$, $30\,\mathrm{L/min}$ and $38\,\mathrm{L/min}$.

4.2. Measurement and correction of optical disturbances in supply flow

In the following, BOS measurements are presented, from which the light deflection δx is determined and $\frac{\partial \xi_x}{\partial x}$ calculated according to Eq 4. Subsequently, Eq. 13 is used to correct the averaged flow velocity.

Fig. 5 shows exemplarily a recorded BOS image, which indicates linear structures in x-direction in the fluid flow surface resulting in pronounced light deflections in y-direction.

The deflection-based 2d displacements of the dot-pattern obtained from the BOS measurements for the three volume flows of $25\,\mathrm{L/min}$, $30\,\mathrm{L/min}$ and $38\,\mathrm{L/min}$ are shown in Fig. 6. In the core area ($y = -8.5\,\mathrm{mm}$ to $8.5\,\mathrm{mm}$), the displacements in x-direction range from $\Delta x = -0.15\,\mathrm{mm}$ to $0\,\mathrm{mm}$, indicating displacements in the negative x-direction. The progression for the respective volume flows are similar to each other with an increase in the slope for higher volume flows. This indicates a change in the jet geometry, which occurs from either increasing surface curvatures or an additionally tilt out of the observation plane.

In the y-direction, dominant displacements are observed, which indicate a pronounced surface curvature. This pronounced surface curvature complicates the BOS measurements, since too strong changes of the surface lead to total reflections. For higher velocities, the curvature decreases slightly, which can be attributed to increased fluctuation of the time-averaged surface. Even
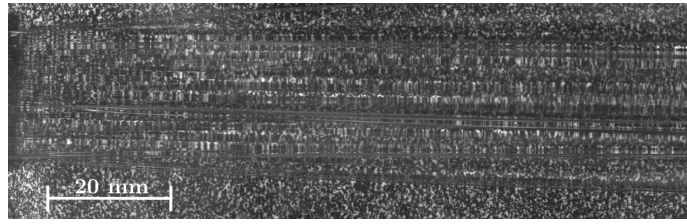
Figure 5. Recording of the BOS measurement for the liquid flow generated with a volume flow of $Q = 30\,\mathrm{L/min}$ at a distance between reference-pattern and liquid of $z_0 = 5\,\mathrm{mm}$.

though the deflections in the y-direction are significantly more prominent than those in the x-direction, they are neglected in the following for the correction of the PIV measurements, since the velocity fields have a negligible velocity y-component (see also section 2).
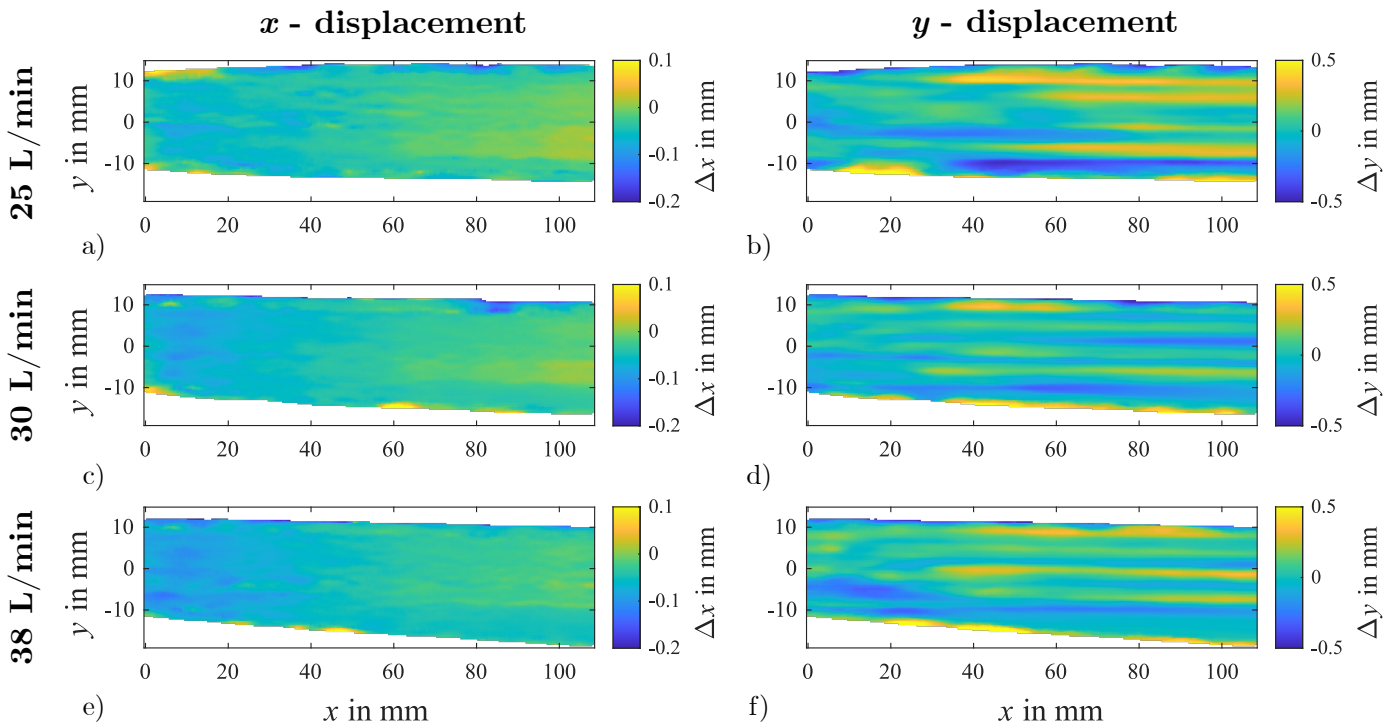

Figure 6. Recording of the BOS measurement for the liquid flow generated with a volume flow of $Q = 25\,\mathrm{L/min},\ 30\,\mathrm{L/min}$ and $38\,\mathrm{L/min}$.

Lastly, the caused systematic measurement deviations from light refraction on the PIV measurements are determined with Eq. 4 in combination with the averaged velocities. A correction of the averaged velocities is calculated with Eq. 13. The results of the uncorrected and corrected velocities for the volume flows of $25\,\mathrm{L/min}$, $30\,\mathrm{L/min}$ and $38\,\mathrm{L/min}$ are shown in Fig. 7.

Two crucial differences can be seen between the corrected and uncorrected velocities: Firstly, the corrected velocities are up to $0.6\,\mathrm{m/s}$, and secondly, the velocity increase along the x-axis has changed to a velocity decrease, which is physically plausible. The correction is in the order of up to $2\,\%$, which is negligible for the cooling process in grinding, but leads to a physically correct qualitative understanding of the flow behaviour.
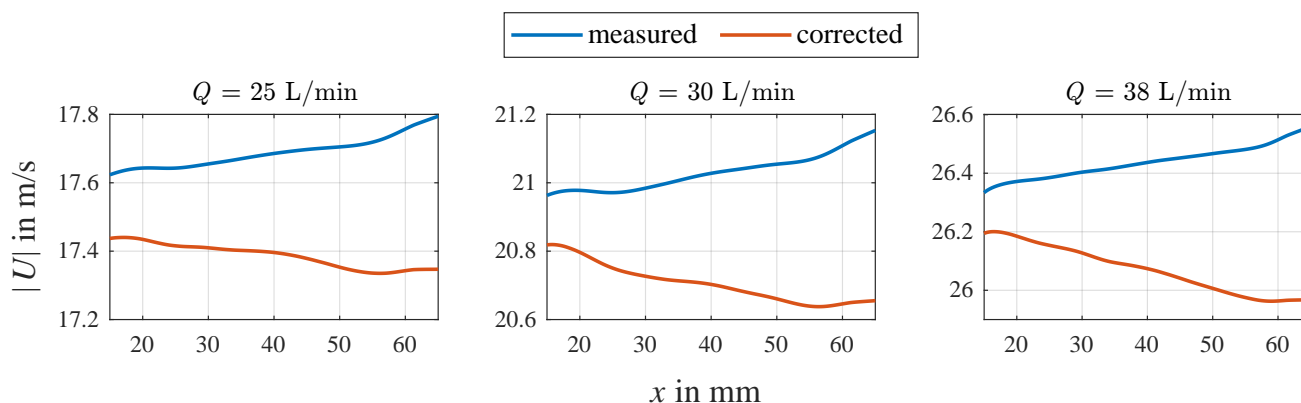
Figure 7. Measured(blue) and corrected(red) average flow velocities for the volume flows of $Q = 25 \, \text{L/min}, \; 30 \, \text{L/min}$ and $38 \, \text{L/min}$.

4.3. Flow measurements of coolant-grinding wheel interaction

For the flow field measurements with the fluid-tool interaction, PIV measurements of the coolant flow for volume flows of $25 \, \text{L/min}$, $30 \, \text{L/min}$ and $38 \, \text{L/min}$ are conducted. A velocity field calculation of the flow before, with and after interaction is achieved based on the illuminated flow structures. Due to the small field of view of $65 \, \text{mm} \times 25 \, \text{mm}$, measurements are conducted for two different positions. The first position is focused on the first interaction of the supply flow with the grinding wheel, whereby the second position is set at the lowest point of the grinding wheel (which is set as the origin $x = y = 0 \, \text{mm}$), to observe the flow behaviour while and after interaction with the tool. The positions are displaced by $30 \, \text{mm}$ to each other and the field of views are overlapping. To give insight of the appearance of the visualised flow in interaction with the grinding wheel, composed images of both positions for the different volume flow rates are shown in Fig. 8. In contrast to the observation of scattered light from small particles as it is used for PIV, the laser light is reflected, refracted or scattered on the flow structures. In this way, the flow structures become visible in the camera images. Thus, the velocity calculation is based on flow structures on the surface instead of particles inside of the liquid and no particle displacement error occurs, which is in contrast to the flow measurement in the free jet flow region. The velocity calculation is based on the classic PIV approach, where the velocity results from displacements in small evaluation areas, that are determined with the digital image cross correlation of double image exposures with known time gap. Results of the calculated average velocity magnitudes of the 2d flow field $|U|$ are shown for both perspectives in Fig. 9. The velocity magnitude is displayed as a colour-coded background and the flow direction indicated by the vector directions. The measurements from first position range go from $x = -67 \, \text{mm}$ to $-3 \, \text{mm}$ and for the second from $x = -37 \, \text{mm}$ to $27 \, \text{mm}$, resulting in an overlap of $x = -37 \, \text{mm}$ to $-3 \, \text{mm}$. For further analysis the areas of 'supply' (before tool-liquid interaction), 'impact' (first tool-liquid interaction) and 'entrainment' (liquid partly adherent on grinding wheel) are defined.

In order to evaluate the impact of light refraction and the validity of the correction on the PIV results from Sec. 4.2, the results are compared with those of the surface structure based velocity.
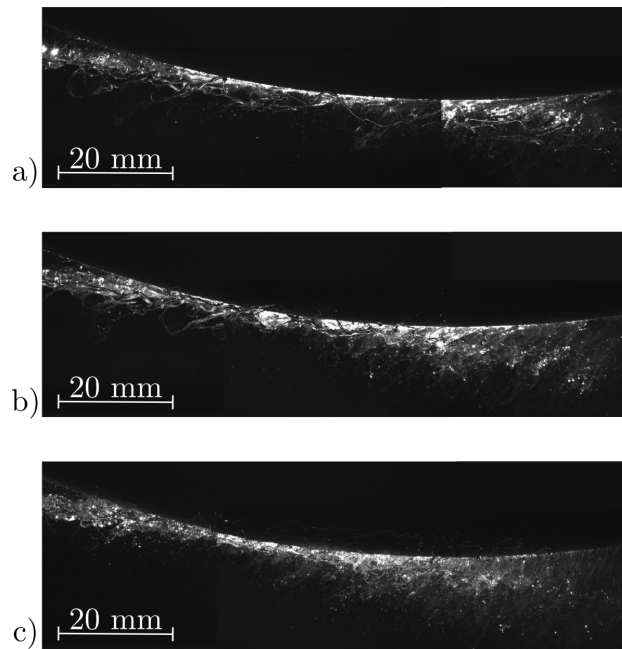
Figure 8. With PIV visualised flow of the coolant in interaction with the grinding wheel. Images from both views are composed. Figure a) to c) are for a supply flow of $Q = 25\,\text{L/min},\ 30\,\text{L/min}$ and $38\,\text{L/min}$.

For this purpose, the velocities $|U_{\text{dis}}|$ of the optical distorted and $|U_{\text{cor}}|$ corrected at the position $x = 60\,\text{mm}$ are listed in Tab. 1. To determine the velocity of the supply flow based on flow structures, the supply range is to be assigned to the region of $x = -65\,\text{mm}$ to $-55\,\text{mm}$. The measured velocity in this area will be defined as velocity based on structures $|U_{\text{str}}|$ and is listed in Tab. 1. The determined velocities are separated by a maximum of $0.6\,\text{m/s}$, which is in the same order as the correction contribution. Furthermore, the corrected velocities are closer to the velocities from the evaluation with the surface structures, which is an indication of a valid correction.

Table 1. Velocities of the supply flow of the optical distorted, corrected PIV measurement, based on flow structures and difference between corrected and based on flow structures for the volume flows of $Q = 25\,\text{L/min},\ 30\,\text{L/min}$ and $38\,\text{L/min}$.

Q in L/min	$|U_{\text{dis}}|$ in m/s	$|U_{\text{cor}}|$ in m/s	$|U_{\text{str}}|$ in m/s	$|U_{\text{cor}}| - |U_{\text{str}}|$ in m/s
25	17.76	17.34	17.38	-0.04
30	21.11	20.65	20.54	0.11
38	26.51	25.96	25.75	0.21

The region of impact is defined as the area in which the supplied fluid initially interacts with the grinding wheel. A decrease in velocity from the impact and change in direction of the fluid are likely to observe, until the fluid gets entrained. The area can be specified as $x = -55\,\text{mm}$ to $-35\,\text{mm}$. Decreased velocities up to $1\,\text{m/s}$ for all volume flows are observed, which are minor in comparison to the inflow velocity and indicate a good transition from supply to entrained flow. Another aspect is given by its shape. As shown in Fig. 8, the cross-section of the supply flow is significantly thicker
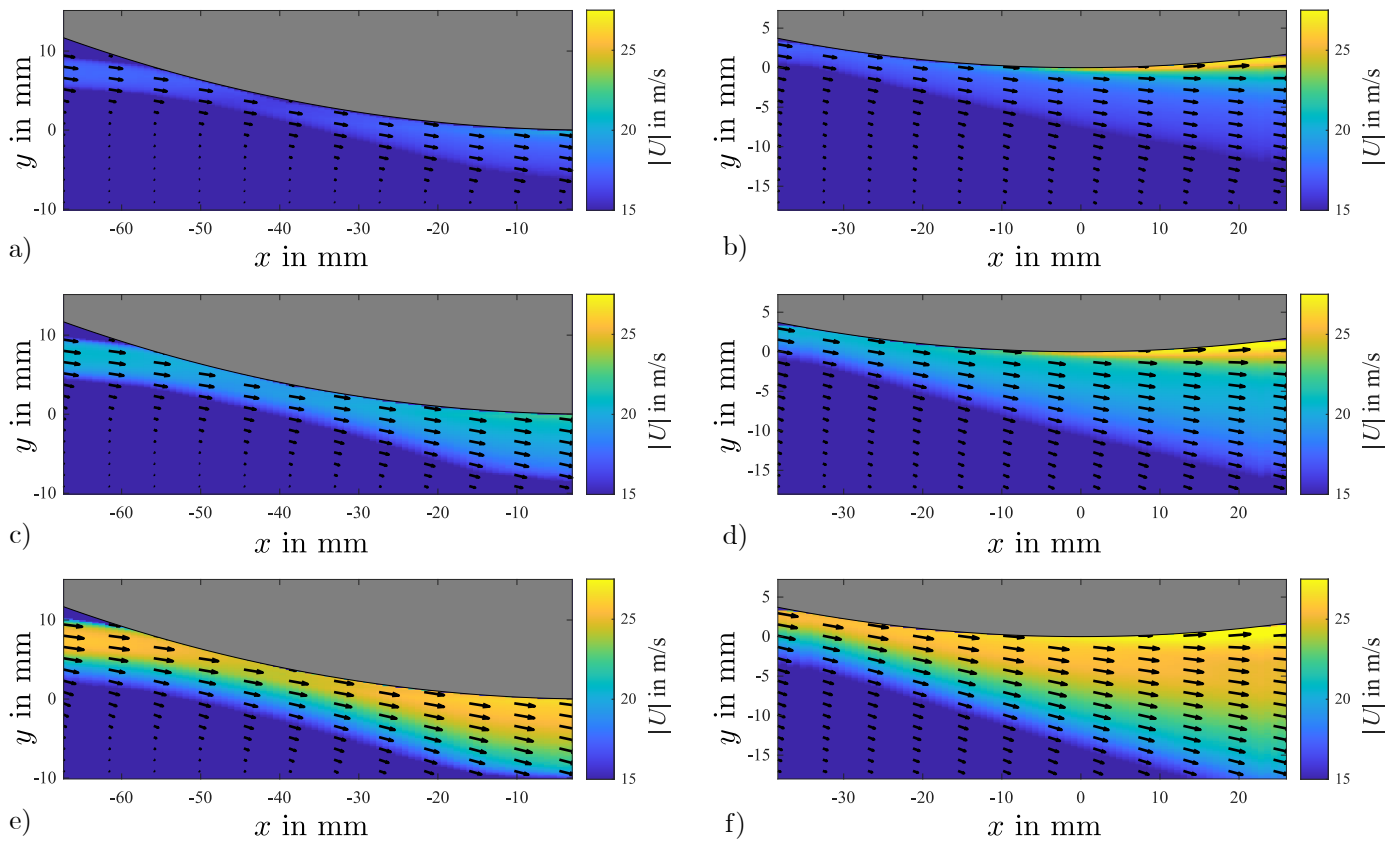
Figure 9. Velocity fields measured with PIV. Supply flow range from top to bottom from $Q = 25\,\text{L/min},\ 30\,\text{L/min}$ and $38\,\text{L/min}$ for the area of interaction (left) and entrainment (right). The position of the grinding wheel is added to the image in grey for clarification.

which tapers with progression. This describes the transition from the free jet into the grinding process, where the liquid is pushed together by the wall of the grinding wheel.

The area of impact passes seamlessly into the area of entrainment, where an acceleration of the flow occurs and applies for the remaining area. After the impact, the flow is in direct contact with the grinding wheel and partly adheres to it. Due to the adhesion, the liquid gets accelerated according to the circumferential velocity of the grinding wheel, while part of the liquid loses its adhesion to the surface. Regardless of the volume flows, a significant increase in velocity is indicated in the area $x > 0\,\text{mm}$, which shows a strong shear flow in the range of $y > 0\,\text{mm}$. Maximum velocities of $26.54\,\text{m/s}$, $27.45\,\text{m/s}$ and $27.93\,\text{m/s}$ are measured for the volume flows of $25\,\text{L/min}$, $30\,\text{L/min}$ and $38\,\text{L/min}$ respectively. This is noteworthy as the circumferential velocity is set to $35\,\text{m/s}$ and demonstrates that the liquid is not accelerated to the maximum velocity, especially not at the lowest point of the grinding wheel, where the grinding process would take place. Furthermore, the velocities for all three volume flows are accelerated to almost the same final value, which is not to be foreseen. The interaction of the liquid with the grinding wheel shows, that the adherence of the liquid to the grinding wheel is predominantly a matter of transporting the coolant, rather than accelerating it. This suggests that the cooling performance is less derived from the supply velocity of the coolant, but rather from the mass flow.

5. Conclusions

In this study, a measurement approach for the determination of the light refraction affecting PIV flow measurements of a highly turbulent two phase liquid flow are presented. Systematic measurement deviations caused by light refraction of the two-phase flow are determined and and used for a correction of the obtained velocity field. Furthermore, measurements of the whole coolant flow of a cooling process in a conventional grinding machine are presented, demonstrating the capability of the PIV measurement technique in this highly turbulent flow. The velocity fields provide information about the flow behaviour of the coolant in interaction with the grinding wheel, resulting in a more detailed characterisation of the area of supply, impact and entrainment and acquire extensive insight of the cooling process in grinding.

For the measurements of the supply flow, the velocity determination is based on flow tracers and therefore suffers from optical distortions. A measurement approach based on the BOS technique in combination with assumptions about the jet geometry provides a quantification and subsequently correction of the velocities. Due to the refraction of light, a slight increase of 1% of the velocities in the core jet area has been measured, which is implausible. With the correction of the velocity, an absolute correction of up to 2% has been applied, resulting in a small decrease in velocity. Although the differences are not significant for the characterisation of the cooling process, the correction reveals a phenomenologically different flow behaviour, which is physically reasonable.

The measured velocity flow fields in interaction with the grinding wheel are based on flow structures rather than particles. A comparison of the obtained flow measurements of those based on flow tracers are in good agreement to the corrected supply flow measurements based on flow tracers, indicating a proper correction. The velocity fields of different volume flows allow a characterisation of the flow in interaction with the grinding wheel. It turned out that a coupling of the fluid with the grinding wheel has much less effect on the flow velocity as supposed. The fluid is not accelerated to the circumferential velocity of the grinding wheel. In addition, despite greatly differing supply velocities, almost identical final velocities are reached by the acceleration of the grinding wheel. This suggests that the cooling performance is less derived from the supply velocity of the coolant, but rather from the mass flow.

The obtained results prove the feasibility of quantitative PIV-based flow velocity field measurements for the supply flow as well as for the liquid-tool interacting flow. This is a key step to the future understanding of the connection between the cooling properties of fluid dynamics and thus, to the ongoing development of optimised cooling in the grinding process.

In future investigations, the influence of a workpiece on the measurability of the flow directly in front of and behind the interaction zone has to be examined. For this purpose, a grinding setup with variable grinding gap will be used. When the fluid interacts with the grinding gap, not all of the fluid is coupled into the cooling process and the non-coupled portion bounces off the workpiece and tool. This results in a highly atomised backflow that affects the observation of the flow and its impact on the flow measurement results is unknown yet.

Funding

References

Brinksmeier, E., Aurich, J. C., Govekar, E., Heinzel, C., Hoffmeister, H.-W., Klocke, F., Peters, J., Rentsch, R., Stephenson, D. J., Uhlmann, E., Weinert, K., and Wittmann, M. (2006). Advances in modeling and simulation of grinding processes. *CIRP Annals*, 55(2):667–696.

C. Vanselow and A. Fischer (2018). Influence of inhomogeneous refractive index fields on particle image velocimetry. *Optics and Lasers in Engineering*, 107:221–230.

Elsinga, G. E., van Oudheusden, B. W., and Scarano, F. (2005). Evaluation of aero-optical distortion effects in piv. *Experiments in Fluids*, 39(2):246–256.

Espenhahn, B., Schumski, L., Vanselow, C., Stöbener, D., Meyer, D., and Fischer, A. (2021). Feasibility of optical flow field measurements of the coolant in a grinding machine. *Applied Sciences*, 11(24):11615.

Gao, Z., Radner, H., Büttner, L., Ye, H., Li, X., and Czarske, J. (2021). Distortion correction for particle image velocimetry using multiple-input deep convolutional neural network and hartmann-shack sensing. *Optics express*, 29(12):18669–18687.

Gomit, G., Chatellier, L., Calluaud, D., and David, L. (2013). Free surface measurement by stereo-refraction. *Experiments in Fluids*, 54(6):1–11.

Heinzel, C., Kirsch, B., Meyer, D., and Webster, J. (2020). Interactions of grinding tool and supplied fluid. *CIRP Annals*, 69(2):624–645.

Kumar, S. S., Karn, A., Arndt, R. E. A., and Hong, J. (2017). Internal flow measurements of drop impacting a solid surface. *Experiments in Fluids*, 58(3).

Meyer, D. and Wagner, A. (2016). Influence of metalworking fluid additives on the thermal conditions in grinding. *CIRP Annals*, 65(1):313–316.

Minor, G., Oshkai, P., and Djilali, N. (2007). Optical distortion correction for liquid droplet visualization using the ray tracing method: further considerations. *Measurement Science and Technology*, 18(11):L23–L28.

Moisy, F., Rabaud, M., and Salsac, K. (2009). A synthetic schlieren method for the measurement of the topography of a liquid interface. *Experiments in Fluids*, 46(6):1021–1036.

Ng, I., Kumar, V., Sheard, G. J., Hourigan, K., and Fouras, A. (2011). Experimental study of simultaneous measurement of velocity and surface topography: in the wake of a circular cylinder at low reynolds number. *Experiments in Fluids*, 50(3):587–595.

Richard, H. and Raffel, M. (2001). Principle and applications of the background oriented schlieren (bos) method. *Measurement Science and Technology*, 12(9):1576–1585.

Schumski, L., Guba, N., Espenhahn, B., Stöbener, D., Fischer, A., and Meyer, D. (2022). Characterization of the interaction of metalworking fluids with grinding wheels. *Journal of Manufacturing and Materials Processing*, 6(3):51.

Vanselow, C., Espenhahn, B., Schumski, L., Stöbener, D., Meyer, D., and Fischer, A. (2021). Flow field measurement of the cooling lubricant supply at the grinding wheel. *tm - Technisches Messen*, 88(12):785–794.

Wu, Y., Liu, Y., Shao, S., and Hong, J. (2019). On the internal flow of a ventilated supercavity. *Journal of Fluid Mechanics*, 862:1135–1165.